





RESEARCH ARTICLE | FEBRUARY 16 2024

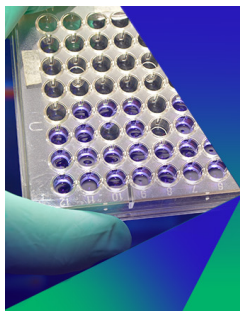
Low-temperature Raman studies of graphene oxide: Analysis of structural properties

A. Glamazda   ; A. Linnik; O. Lytvyn  ; V. Karachevtsev 

 Check for updates

AIP Advances 14, 025033 (2024)

<https://doi.org/10.1063/5.0188838>



Biomicrofluidics

Special Topic:
Microfluidics and Nanofluidics in **India**

Submit Today



Low-temperature Raman studies of graphene oxide: Analysis of structural properties

Cite as: AIP Advances 14, 025033 (2024); doi: 10.1063/5.0188838

Submitted: 27 December 2023 • Accepted: 17 January 2024 •

Published Online: 16 February 2024



View Online



Export Citation



CrossMark

A. Glamazda,^{1,a)}  A. Linnik,¹ O. Lytvyn,²  and V. Karachevtsev¹ 

AFFILIATIONS

¹B. Verkin Institute for Low Temperature Physics and Engineering of NAS of Ukraine, 47 Nauky Ave., Kharkiv 61103, Ukraine

²Borys Grinchenko Kyiv University, 18/2 Bulvarno-Kudriavska Str., Kyiv 04053, Ukraine

^{a)}Author to whom correspondence should be addressed: glamazda@ilt.kharkov.ua

ABSTRACT

This work is devoted to the low-temperature Raman studies of a bright representative of 2D materials—graphene oxide (GO) film in the range of 5–325 K. The performed analysis of the temperature evolution of the peak positions as well as linewidths of two Raman modes D ($\sim 1300\text{ cm}^{-1}$) and G ($\sim 1600\text{ cm}^{-1}$) was described in terms of the anharmonic model. The temperature behavior of the G mode demonstrated a slight deviation from the anharmonic model below $\sim 50\text{ K}$ in contrast to the D mode, which could be explained by involving an additional phonon decay channel. The analysis of the linewidth of the Raman modes showed that the distribution of defects in GO is inhomogeneous and surface functionalization effectively separates neighboring layers. The average value of the distance between defects and the defect density was estimated. The obtained results can be useful for understanding phonon dynamics for the development of nanodevices based on 2D materials where confinement of propagation of phonon excitations plays a key role.

© 2024 Author(s). All article content, except where otherwise noted, is licensed under a Creative Commons Attribution (CC BY) license (<http://creativecommons.org/licenses/by/4.0/>). <https://doi.org/10.1063/5.0188838>

I. INTRODUCTION

The carbon low-dimensional materials are a new class that can change the approach in the development and design of the novel element base for advanced technologies and electronic devices. For such materials, a number of requirements are put forward, which are related to their homogeneity and the possibility to tune the electrical properties and change the carrier density. Graphene is a two-dimensional sp^2 -hybridized carbon monolayered nanomaterial with a “honeycomb” lattice structure. This structure has a high tensile strength and a large surface area.¹ The honeycomb surface gives rise to many new physical effects that can find applications in areas such as quantum magnetism, electronics, etc.^{2,3} The carbon 2D monolayer has a number of unique physical characteristics, such as an extremely high surface/mass ratio, high thermal conductivity (almost ten times higher than the thermal conductivity of copper), optical transparency in the visible range of about $\sim 97\%$, high electronic mobility, etc.⁴ Studying the properties of graphene is relevant in view of many potential applications of this material. Chemical modification of the graphene surface leads to new interesting physicochemical properties. For example, oxidation of the graphene surface with covalently linked different types

of oxygen-containing functional groups (epoxy, hydroxyl, carboxyl) introducing sp^3 defects changes the optoelectronic properties of graphene and gives rise to a bandgap between its valence and conduction bands with width depending on the number of defects on the surface.⁵ The modified graphene material is called graphene oxide (GO). The linked oxygen-containing functional groups can serve as anchors for the further multi-stage process of functionalization of graphene. Thus, it is very important to certify the individual components of nanohybrids for defects that can significantly change the physical properties of nanohybrids through the appearance of the inputting barrier limiting the wave propagation. The low-temperature studies shed light on the quantum effects suppressed due to thermal fluctuation at room temperature. The low-temperature Raman study gives an understanding of the phonon dynamics because the phonons play an essential role in thermal conductivity and mechanical properties of materials, as well as they can couple to other excitations that significantly expand the field of their study.

The low-temperature dynamics of Raman spectra of graphene-related materials has been studied before, but the comparison of the obtained results is a nontrivial task since the investigated materials have different defect stages and surrounding, and the spectra

were obtained in different temperature ranges.^{6–12} It was found that the substrate on which the material was deposited or grown plays an essential role since the two-dimensional material is very tightly bound to the substrate. In addition, the graphene family includes nanomaterials with different amounts of oxidation groups and defects that affect Raman spectra. Therefore, at present, the expansion of low-temperature spectral experiments in this field is necessary to obtain a complete picture of phonon dynamics in graphene nanomaterials.

In this work, we focus on the Raman studies of phonon properties of the GO film in the range of 5–325 K. Previously, the low-temperature vibrational properties of the GO films have not been studied within this temperature range. The functionalization of the graphene remains one of the most common methods for its promotion in practical applications as well as a cost effective approach for producing single graphene layers. Identifying all the associated factors that can affect the transport and thermal properties of the GO material is an important task in the development of electronic devices based on it. We have performed the analysis of the temperature evolution of the two most intensive Raman fingerprint bands: defect-induced forbidden D mode and the G mode related to the C=C vibrations. The present bands are very

sensitive to the structural distortion and inhomogeneities on the carbon surface. On analyzing temperature-dependent Raman spectra of the GO films, we have revealed the shifts of Raman modes and decrease in linewidths upon cooling that was discussed in terms of phonon anharmonicity. The anomalous low-temperature dynamics of the phonon bands was explained by involving an additional phonon decay channel. The comparative analysis of Raman spectra of graphene-related materials and the data taken within the frameworks of the present work was performed.

II. DETAILS OF THE EXPERIMENT

The water-soluble graphene oxide was prepared using the modified Hummers method in accordance with the recently published methodology in Ref. 13. The suspension of graphene oxide was precipitated on a fused quartz substrate and dried under hot air-drying conditions at about 40 °C. The fused quartz has a low coefficient of thermal expansion that may reduce the stress in the precipitated film induced by the substrate. The performed analysis of Raman studies of the graphene-related materials showed that the crystalline substrate (mica, silicon, etc.) can stimulate the appearance of additional

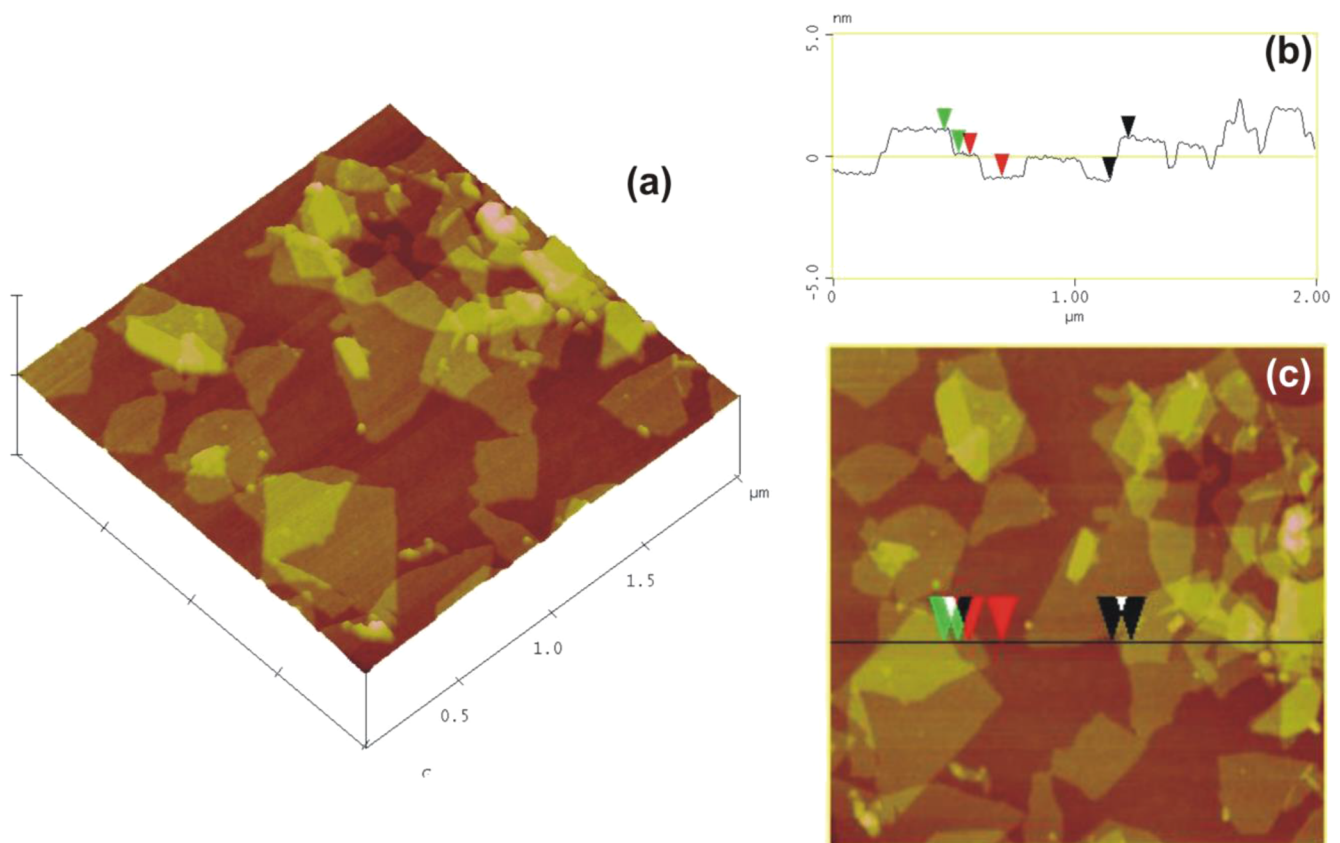


FIG. 1. (a) 3D AFM image of the GO layers adsorbed on freshly cleaved mica. (b) 2D AFM image of the GO layers adsorbed on freshly cleaved mica. (c) The cross-section profile corresponds to the black line drawn in the image. The heights of the GO layers were measured between triangles.

stress in the layered material and is of particular interest. However, the study of this effect was not within the aim of the present work.

The Raman experiments were carried out with the 632.8 nm (1.96 eV) laser excitation from a He–Ne laser in the 90°-polarized configuration. The laser power per unit area of the film was less than 0.7 mW/mm² to avoid the local overheating of the sample. The scattered light was detected with a cooled CCD camera. The low-temperature investigations were performed in an optical cryostat in helium vapors.

The morphology of the GO surfaces was studied with Atomic Force Microscopy (AFM). The aqueous suspensions of GO are used to prepare samples for the AFM measurements. 7 μl of a dilute (1:100) suspension is placed onto a freshly cleaved mica surface by the spin coating method. The sample is then air-dried and analyzed by AFM. AFM images of GO are obtained using a Nanoscope III D3000 AFM (Digital Instruments, Santa Barbara, CA) operating in the tapping mode.

III. RESULTS AND DISCUSSION

A. Nanoflakes of GO by AFM study

AFM experiments were performed to estimate the size of the GO layers and to determine the average number of layers that prevailed in our samples. Figure 1(a) shows the 3D AFM image of the GO layers produced in the present study and adsorbed to freshly cleaved mica. It can be seen in the figure that the separated layers of the GO sample have different sizes located on top of the other. Figure 1(b) shows a 2D AFM image. We have analyzed the height of the precipitated GO layers along the black line. The thickness of the

GO layers was measured between the identical triangles presented in the same color. The average thickness of the single GO layers is about 0.87 nm as shown in the cross-section profile in Fig. 1(c). This value indicates that on mica mainly GO monolayers are adsorbed that agrees with the previous reports.^{13,14} The thickness value of about 1.75 nm (taken between black triangles) indicates the overlapping of two monolayers while the double layers can also be observed. The height measurements performed at different locations indicate that the GO layers have a uniform thickness (without any noticeable wrinkles).

B. Low-temperature Raman studies of GO film

Figure 2 shows the evolution of the temperature-dependent Raman spectra of GO from 5 to 325 K. Raman spectra observed in the range of 1100–1700 cm⁻¹ contain two intensive bands located at about 1330 and 1600 cm⁻¹, the D and G bands, respectively.¹⁵ For a detailed analysis of the temperature evolution of the observed phonon bands, the observed Raman spectra were fitted with a sum of Lorentzians. The methodology of the GO Raman spectrum fitting is quite diverse. The fitting of the band assigned to the tangential mode with two contours can be used for the estimation of the

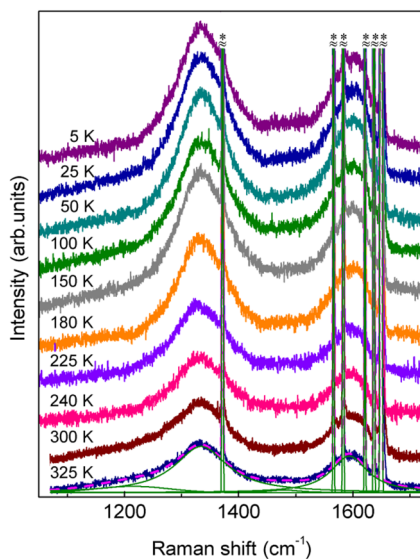


FIG. 2. The evolution of the temperature-dependent Raman spectra of GO. There are intensive sharp plasma lines marked with asterisks from the He–Ne-laser in the spectra. They were used for energy calibration of the spectrometer. The spectra were fitted by a sum of the Lorentzian profiles. The magenta dashed line represents the total sum of a fitting, and the thin green lines represent the deconvolution of the GO Raman spectrum taken at 325 K.

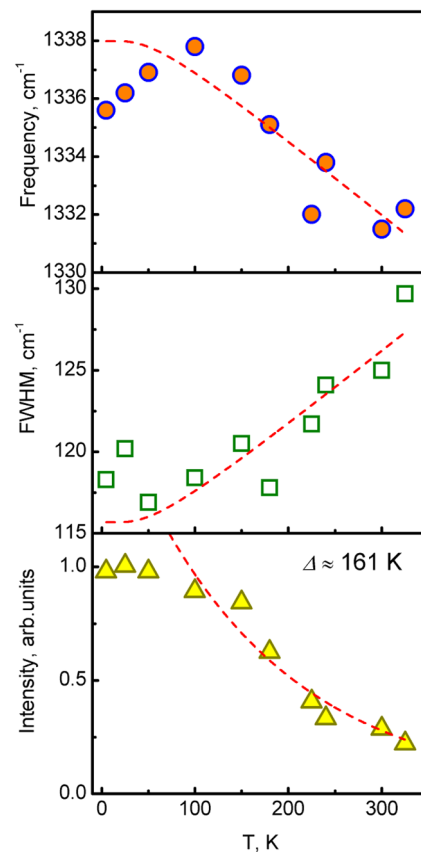


FIG. 3. The temperature dependence of the frequencies, FWHM, and intensity of the defect-activated mode at 1330 cm⁻¹. The dashed red lines are a fit to an anharmonic model.²² The Bose corrected phonon intensity is a fit to $I(T) \sim \exp(-k_B T/\Delta)$.

C/O atom ratio.¹⁶ In this fitting, the difference between the peak positions of two bands increases with the growth of the C/O atom ratio. We see no justifications for the fitting of the G-mode with two contours: tangential mode has an almost symmetric shape. Therefore, we have used the minimal number of Lorentzians for the decomposition of the bands presented in Raman spectra. The temperature behavior of the parameters of the D and G bands is presented in Figs. 3 and 4. These figures show the temperature-dependent evolution of the peaks at 1330 and 1600 cm^{-1} , linewidths, and their integral intensities. It should be noted that the linewidths of the D and G-modes are larger in comparison to recently published Raman data of graphene,^{12,17} which can be explained by the inhomogeneous distribution of the defects on the GO surface confining the phonon propagation^{18,19} as well as the pressure/strain induced by the neighboring layers in multilayered precipitation of the GO layers.²⁰ Also, we suppose that the inhomogeneous defect distribution can produce a deformation of the GO surface, which in turn would lead to the band broadening. As is known, to describe the temperature evolution of the band peak and linewidth correctly, we should take into account phonon–phonon and electron–phonon interactions.²¹ GO film has a low electric conductivity, and thus

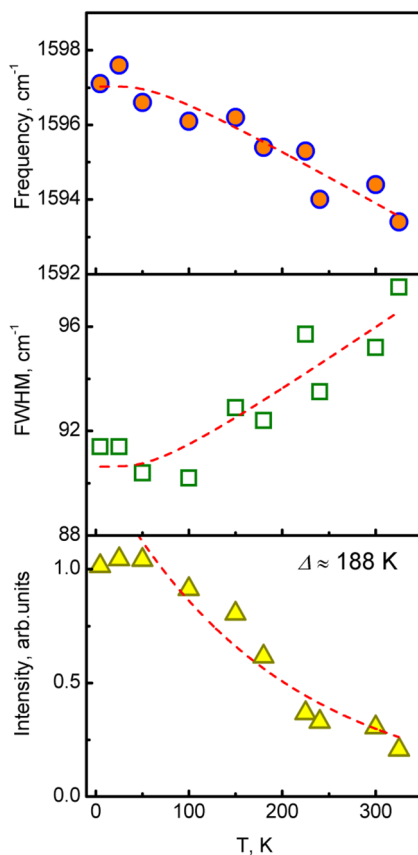


FIG. 4. The temperature dependence of the frequencies, full widths at the half maximum (FWHM), and intensity of the modes at 1590 cm^{-1} . The dashed red lines are a fit to an anharmonic model.²² The Bose corrected phonon intensity is a fit to $I(T) \sim \exp(-k_B T/\Delta)$.

the electron–phonon contribution is neglected in the linewidth of observed Raman bands. Therefore, we will fit the experimental data with the temperature behavior of the band peak and linewidth using the model involving the phonon decay channel only. The temperature-dependent peak energy is described in terms of the simplified anharmonic model considering only three-phonon decay processes²²

$$\omega(T) = \omega_0 + A \left[1 + 2/(e^x - 1) \right], \quad (1)$$

where ω_0 is the harmonic frequency of the optical mode while T approaches 0 K, $x = \hbar\omega_0/(2k_B T)$, \hbar is the reduced Planck's constant, k_B is Boltzmann's constant, and A is a constant for the three-phonon decay processes. In a similar manner to the fitting peak positions with Eq. (1), the full width at half maximum (FWHM) is described by

$$\Gamma(T) = \Gamma_0 + B \left[1 + 2/(e^x - 1) \right], \quad (2)$$

where Γ_0 is the FWHM at $T = 0$ and B is constant.²² As evident from Figs. 3 and 4, the lattice anharmonicity provides a reasonable description of the temperature dependence of the phonon frequencies and FWHM of the G-mode (see the dashed red lines in Fig. 4). The description of the temperature behavior of the D-mode is entangled with the anharmonic model, i.e., it demonstrates reasonable approximation from room temperatures down to about 50 K where some deviation from the model is observed. We suppose that below 50 K the additional phonon decay channel appears.¹² According to Eq. (1), for a reasonable fitting of the experimental data presented in Fig. 3, the parameters $\omega_0 = 1339.9 \text{ cm}^{-1}$ and $A = -2.00$ for the D mode, and $\omega_0 = 1598.3 \text{ cm}^{-1}$ and $A = -1.31$ for the G mode were used. The fitting of the temperature behavior of linewidths for D and G modes by Eq. (2) was performed with the parameters $\Gamma_0 = 112.2 \text{ cm}^{-1}$ and $B = 3.52$ for the D mode, and $\Gamma_0 = 88.4 \text{ cm}^{-1}$ and $B = 2.24$ for the G mode.

The fitting of the linear regions of the peak positions of the G and D modes as well as FWHM of both bands in the range of 50–325 K gives the estimation of a temperature coefficient (TC). The peak positions of the G and D modes exhibit negative linear TC equal to -0.012 and $-0.028 \text{ cm}^{-1}/\text{K}$, respectively. The calculated TCs of the studied sample, in general terms, are comparable to the TC values for graphene-related materials presented in Table I. However, the comparative analysis of our data and results reported by other authors is not trivial because of different synthesis processes of GO, possible difference in defects' types and defect density, temperature range within the measurements that were carried out, and crystallite size.^{8,9,23} With detailed consideration of the data presented in Table I, we can conclude that taken TCs for GO studied in the present work are close to TCs for rGO powder.¹⁹ The functionalization of the graphene surface may facilitate increasing the interlayer spacing and decreasing stress induced by the neighboring layers in the precipitated film. A similar effect was observed in low-temperature studies of single-walled carbon nanotubes wrapped by DNA.^{24,25}

The linewidths of the D and G modes of our sample show positive TCs equal to 0.044 and $0.027 \text{ cm}^{-1}/\text{K}$, respectively. The taken values of TCs differ from recently published for exfoliated single and few-layered graphene.^{12,19,26,27} This behavior can be explained by the fact that the layering of neighboring monolayers forms an

TABLE I. The comparison of the calculated temperature coefficients (TCs) for graphene-related materials with the data taken in the present work.

Graphene-related material	T, K	TC, cm ⁻¹ /K	References
Unsupported vertical graphene sheets were grown on SiC substrates	79–773 K	TC (ω_G) = -0.020 cm ⁻¹ /K (79–400 K); TC (ω_G) = -0.022 cm ⁻¹ /K (400–773 K); TC(Γ_G) demonstrates quasi-continuous behavior in the temperature range of about 5–300 K	7
Few-layered graphene grown on the copper foil and fixed on 4H-SiC substrate	80–500 K	TC (ω_G) = -0.0257 cm ⁻¹ /K for the one-layered graphene; TC (ω_G) = -0.0189 cm ⁻¹ /K for the two-layered graphene	29
The mechanically exfoliated graphene on the Si {100} substrate covered with an 89-nm SiO ₂	77–318 K	TC (ω_G) = -0.0156 cm ⁻¹ /K for the defect-free 1–10 graphene layers; TC (ω_G) = -0.0252 cm ⁻¹ /K for the defective 1–10 graphene layers after ion C+ bombardment; TC (Γ_G) ≈ 0 cm ⁻¹ /K for the defect-free and defective set	12
Single-layered graphene prepared by the mechanical exfoliation of graphite and fixed on glass slides	77–673 K	TC (ω_G) = -0.016 cm ⁻¹ /K; TC (Γ_G) ≈ 0 cm ⁻¹ /K	26
rGO powder	173–723 K	TC (ω_D) = -0.010 cm ⁻¹ /K; TC (ω_G) = -0.009 cm ⁻¹ /K; TC (Γ_D) = 0.005 cm ⁻¹ /K; TC (Γ_G) ≈ 0 cm ⁻¹ /K	19
Graphene flakes micromechanically cleaved of bulk graphite crystals and on SiO ₂ /Si substrate with SiO ₂ thickness as 90 nm	–190–200 °C	TC (ω_G) = -0.02519 cm ⁻¹ /°C – 5.187×10^{-6} cm ⁻¹ /°C ² for the graphene flakes with thickness of 16.5 nm; TC (ω_G) = -0.01745 cm ⁻¹ /°C – 7.145×10^{-6} cm ⁻¹ /°C ² for the graphene flakes with thickness of 36.5 nm; TC (Γ_G) = 2.533×10^{-3} cm ⁻¹ /°C for the graphene flakes with thickness of 16.5 nm; TC (Γ_G) = 3.604×10^{-3} cm ⁻¹ /°C for the graphene flakes with thickness of 36.5 nm	27
GO powder dispersed in aqueous suspension and precipitated on a fused quartz	5–325 K	TC (ω_D) = -0.018 cm ⁻¹ /K; (50–325 K); TC (ω_G) = -0.012 cm ⁻¹ /K. (50–325 K); TC (Γ_D) = 0.044 cm ⁻¹ /K; (50–325 K); TC (Γ_G) = 0.027 cm ⁻¹ /K. (50–325 K)	The present work

irregular and inhomogeneous layered 3D structure. The irregularity and defectiveness of the formed structure inhibit the phonon propagation along the stacking direction of the layered array of the GO layers. This, in turn, reduces the phonon lifetime and results in the broadening of the phonon bands. The significant difference between TC (Γ_D) and TC (Γ_G) was estimated. A similar effect was revealed when analyzing the Raman spectra of graphene.²⁷

We examine now the temperature-dependent intensity of two bands presented in Figs. 3 and 4. The Bose-corrected intensities of the phonon bands exhibit an exponential-like decay, $I(T) \sim \exp(-k_B T/\Delta)$, with increasing temperature.²⁸ In insulating materials, the phonon intensity $I(T)$ is highly susceptible to changes in the dielectric function concerning the displacement of the normal mode. Thus, reaching a plateau in the intensity growth with the temperature decrease indicates the dielectric function changes below 50–100 K in involving an additional phonon decay channel. The estimation of the threshold value of the activation energy gap (Δ) of the phonon decay channel from analysis of the intensities of the D and G bands gave 161 and 188 K, respectively. The difference between

the two values is explained by the different nature of the origin of the two modes.

C. Structural properties of graphene oxide by Raman spectroscopy

The question targeting to evaluation of the defect degree of nanomaterials is widely discussed in literature. The application of Raman spectroscopy as a non-destructive technique to analyze the structural defect of nanomaterial surface is widely used in practice. For example, for performing the evaluation of the defect degree (L_D) of GO we have analyzed the I_D/I_G ratio, which corresponds to the Raman peak intensity ratio of D- and G-modes.^{30,31} The temperature-dependent variation of the I_D/I_G ratio is presented in Fig. 5. The performed analysis of the I_D/I_G ratio as a function of temperature has revealed a weak dependence with an average value of 1.32. The estimated value of the ratio is enough high that could be explained by the high defectiveness of the GO surface.

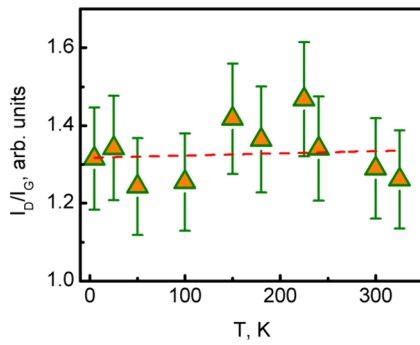


FIG. 5. The temperature dependence of the I_D/I_G ratio. The data were fitted with a linear function demonstrating a weak dependence on the temperature that gives an average value of about 1.32.

The average distance between the defects (L_D) of the present GO material was calculated according to Ref. 31, and its value is dependent on the excitation laser wavelength (λ_L) (dimension is presented in nanometers)

$$L_D^2(\text{nm})^2 = (1.8 \pm 0.5) \times 10^{-9} \lambda_L^4 \left(\frac{I_D}{I_G} \right)^{-1}. \quad (3)$$

By substituting the values of λ_L and I_D/I_G into Eq. (3), we can calculate an averaged L_D equal to about 15 nm. The defect density (n_D) can be calculated using the following equation:³¹

$$n_D(\text{cm})^{-2} = \left(\frac{(1.8 \pm 0.5) \times 10^{22}}{\lambda_L^4} \right) \left(\frac{I_D}{I_G} \right). \quad (4)$$

The defect density (n_D) calculated using Eq. (4) is equal to about $1.5 \times 10^{11} \text{ cm}^{-2}$ for the whole temperature range. The obtained averaged values of L_D and n_D are in good accordance with the previously published studies for graphene-related materials, for example, $L_D \approx 12 \text{ nm}$ and $n_D \approx 2.3 \times 10^{11} \text{ cm}^{-2}$ for rGO;¹⁹ $L_D \approx 35.32\text{--}13.69 \text{ nm}$ for pristine multilayer graphene and treated with oxygen plasma, respectively;³² L_D changes from 21.8 to 42.9 nm for the pristine graphene films to 15.8–18.2 nm for the nitrogen-doped graphene.³³

The I_D/I_G ratio also can be used for the estimation of the average size of effective in-plane crystallites or graphitic domains (L_a), characterized by coherent phonon scattering³⁴

$$L_a(\text{nm}) = \frac{560}{E_\lambda^4} \frac{1}{I_D/I_G}, \quad (5)$$

where E_λ is the excitation energy of the laser (in eV). The crystallite size estimated by Eq. (5) gives L_a equal to about 28 nm. A closer look at the AFM image of the GO layers presented in Fig. 1(a) gives grounds to speak that, on average, about 1000 graphitic domains can be in the GO layer. Of course, this is an important remark that should be used for development of the multifunctional thermally and electrically conductive devices based on graphene oxide material.

IV. CONCLUSION

In this work, we have performed temperature-dependent Raman analysis of the GO layers in the temperature range of 5–325 K. The performed analysis of the linewidths of the Raman fingerprint D- and G-modes taken in the frequency range of 1100–1700 cm^{-1} showed a significant broadening of the bands, which was explained by a confinement of the phonon propagation. The temperature dependence of the peak positions as well as linewidths of the G and D modes was described in terms of the anharmonic model. The temperature behavior of the G mode demonstrates a slight deviation from the anharmonic model below 50 K in contrast to the D mode, which could be explained by involving an additional phonon decay channel. The analysis of the I_D/I_G ratio showed a high defect degree of the GO surface with the average distance between defects equal to about 15 nm and the defect density - $1.5 \times 10^{11} \text{ cm}^{-2}$. The linear size of the graphene domain was estimated at 28 nm. The activation energy gap (Δ) of the phonon decay channel estimated from analysis of the intensities of the D and G bands has values 161 and 188 K, respectively. The difference between the two values is explained by the different nature of the origin of the two modes. The understanding of phonon dynamics plays an important role in the study of carrier transferring in graphene nanomaterials. The results of the present work can be used in the development of electronic nanodevices.

ACKNOWLEDGMENTS

A.G. gratefully thanks Dr. A. Peschanskii and Dr. N. Galtsov (B. Verkin Institute for Low Temperature Physics and Engineering of the National Academy of Sciences of Ukraine) for the interest in the presented work and the valuable discussions. The authors acknowledge financial support from the National Academy of Sciences of Ukraine (Grant No. 0120U100157).

AUTHOR DECLARATIONS

Conflict of Interest

The authors have no conflicts to disclose.

Author Contributions

All authors discussed the results and commented on the manuscript. O. Lytvyn performed AFM characterization. A. Glamazda and A. Linnik carried out Raman measurements and analysis of Raman data. V. Karachevtsev planned and coordinated the project. A. Glamazda and V. Karachevtsev wrote the paper.

A. Glamazda: Conceptualization (equal); Formal analysis (equal); Investigation (equal); Writing – original draft (equal); Writing – review & editing (equal). **A. Linnik:** Formal analysis (equal); Software (equal). **O. Lytvyn:** Data curation (equal); Formal analysis (equal); Writing – review & editing (equal). **V. Karachevtsev:** Conceptualization (equal); Writing – original draft (equal); Writing – review & editing (equal).

DATA AVAILABILITY

The data that support the findings of this study are available from the corresponding author upon reasonable request.

REFERENCES

- ¹M. Krystek, D. Pakulski, V. Patroniak, M. Górski, L. Szojda, A. Ciesielski, and P. Samori, "High-performance graphene-based cementitious composites," *Adv. Sci.* **6**(9), 1801195 (2019).
- ²S. Mishra, D. Beyer, K. Eimre, S. Kezilebieke, R. Berger, O. Gröning, C. A. Pignedoli, K. Müllen, P. Liljeroth, P. Ruffieux, X. Feng, and R. Fasel, "Topological frustration induces unconventional magnetism in a nanographene," *Nat. Nanotechnol.* **15**, 22 (2020).
- ³E. Kogan, "Graphene for electronics," *Nanomaterials* **12**(24), 4359 (2022).
- ⁴A. Armano and S. Agnello, "Two-dimensional carbon: A review of synthesis methods, and electronic, optical, and vibrational properties of single-layer graphene," *C* **5**(4), 67 (2019).
- ⁵N. S. Rajput, S. Al Zadjali, M. Gutierrez, A. M. K. Esawi, and M. Al Teneiji, "Synthesis of holey graphene for advanced nanotechnological applications," *RSC Adv.* **11**, 27381 (2021).
- ⁶I. Calizo, A. A. Balandin, W. Bao, F. Miao, and C. N. Lau, "Temperature dependence of the Raman spectra of graphene and graphene multilayers," *Nano Lett.* **7**(9), 2645 (2007).
- ⁷J. Lin, L. Guo, Q. Huang, Y. Jia, K. Li, X. Lai, and X. Chen, "Anharmonic phonon effects in Raman spectra of unsupported vertical graphene sheets," *Phys. Rev. B* **83**, 125430 (2011).
- ⁸W. Wang, Q. Peng, Y. Dai, Z. Qian, and S. Liu, "Temperature dependence of Raman spectra of graphene on copper foil substrate," *J. Mater. Sci.: Mater. Electron.* **27**, 3888 (2016).
- ⁹J. Judek, A. P. Gertych, M. Krajewski, K. Czerniak, A. Łapińska, J. Sobieski, and M. Zdrojek, "Statistical analysis of the temperature dependence of the phonon properties in supported CVD graphene," *Carbon* **124**, 1 (2017).
- ¹⁰M. S. Tivanov, E. A. Kolesov, O. V. Korolik, A. M. Saad, and I. V. Komissarov, "Effect of the substrate on phonon properties of graphene estimated by Raman spectroscopy," *J. Low Temp. Phys.* **190**, 20 (2018).
- ¹¹H. N. Liu, X. Cong, M. L. Lin, and P. H. Tan, "The intrinsic temperature-dependent Raman spectra of graphite in the temperature range from 4 K to 1000 K," *Carbon* **152**, 451 (2019).
- ¹²M. Yang, L. Wang, X. Qiao, Y. Liu, Y. Shi, H. Wu, B. Liang, X. Li, and X. Zhao, "Temperature dependence of G and D' phonons in monolayer to few-layer graphene with vacancies," *Nanoscale Res. Lett.* **15**, 189 (2020).
- ¹³M. V. Karachevtsev, S. G. Stepanian, A. Y. Ivanov, V. S. Leontiev, V. A. Valeev, O. S. Lytvyn, L. Adamowicz, and V. A. Karachevtsev, "Binding of polycydic acid to graphene oxide: Spectroscopic study and computer modeling," *J. Phys. Chem. C* **121**, 18221 (2017).
- ¹⁴T. Bu, H. Gao, Y. Yao, J. Wang, A. J. Pollard, E. J. Legge, C. A. Clifford, A. Delvallée, S. Ducourtieux, M. A. Lawn, B. Babic, V. A. Coleman, Å. Jämting, S. Zou, M. Chen, Z. J. Jakubek, E. Jacob, N. Chanthawong, K. Mongkolsuttirat, G. Zeng, C. M. Almeida, B.-C. He, L. Hyde, and L. Ren, "Thickness measurements of graphene oxide flakes using atomic force microscopy: Results of an international interlaboratory comparison," *Nanotechnology* **34**(22), 225702 (2023).
- ¹⁵P. T. Araujo, M. Terrones, and M. S. Dresselhaus, "Defects and impurities in graphene-like materials," *Mater. Today* **15**(3), 98 (2012).
- ¹⁶A. A. King, B. R. Davies, N. Noorbehesht, P. Newman, T. L. Church, A. T. Harris, J. M. Razal, and A. I. Minett, "A new Raman metric for the characterisation of graphene oxide and its derivatives," *Sci. Rep.* **6**, 19491 (2016).
- ¹⁷I. Efthimiopoulos, S. Mayanna, E. Stavrou, A. Torode, and Y. Wang, "Extracting the anharmonic properties of the G-band in graphene nanoplatelets," *J. Phys. Chem. C* **124**(8), 4835 (2020).
- ¹⁸S. Osswald, V. N. Mochalin, M. Havel, G. Yushin, and Y. Gogotsi, "Phonon confinement effects in the Raman spectrum of nanodiamond," *Phys. Rev. B* **80**, 075419 (2009).
- ¹⁹M. Sharma, S. Rani, D. K. Pathak, R. Bhatia, R. Kumar, and I. Sameera, "Temperature dependent Raman modes of reduced graphene oxide: Effect of anharmonicity, crystallite size and defects," *Carbon* **184**, 437 (2021).
- ²⁰D. Machon, C. Bousige, R. Alencar, A. Torres-Dias, F. Balima, J. Nicolle, G. de Sousa Pinheiro, A. G. Souza Filho, and A. San-Miguel, "Raman scattering studies of graphene under high pressure," *J. Raman Spectrosc.* **49**, 121 (2018).
- ²¹Z. Han, X. Yang, S. E. Sullivan, T. Feng, L. Shi, W. Li, and X. Ruan, "Raman linewidth contributions from four-phonon and electron-phonon interactions in graphene," *Phys. Rev. Lett.* **128**, 045901 (2022).
- ²²M. Balkanski, R. F. Wallis, and E. Haro, "Anharmonic effects in light scattering due to optical phonons in silicon," *Phys. Rev. B* **28**, 1928 (1983).
- ²³N. Ferralis, "Probing mechanical properties of graphene with Raman spectroscopy," *J. Mater. Sci.* **45**, 5135 (2010).
- ²⁴V. A. Karachevtsev and A. Y. Glamazda, "Raman spectroscopy of DNA-wrapped single-walled carbon nanotube films at 295 and 5 K," *Low Temp. Phys.* **36**(5), 373 (2010).
- ²⁵A. Y. Glamazda, V. S. Leont'ev, A. S. Linnik, and V. A. Karachevtsev, "Luminescence investigations of hybrids of carbon nanotubes with DNA in a water suspension and film at 5–290 K," *Low Temp. Phys.* **34**(12), 1033 (2008).
- ²⁶D. J. Late, U. Maitra, L. S. Panchakarla, U. V. Waghmare, and C. N. Rao, "Temperature effects on the Raman spectra of graphenes: Dependence on the number of layers and doping," *J. Phys.: Condens. Matter* **23**(5), 055303 (2011).
- ²⁷X. Li, J. Liu, K. Ding, X. Zhao, S. Li, W. Zhou, and B. Liang, "Temperature dependence of Raman-active in-plane E_{2g} phonons in layered graphene and h-BN flakes," *Nanoscale Res. Lett.* **13**(1), 25 (2018).
- ²⁸A. Glamazda, K.-Y. Choi, P. Lemmens, W. S. Choi, H. Jeon, T. L. Meyer, and H. N. Lee, "Structural instability of the CoO_4 tetrahedral chain in $\text{SrCoO}_{3-\delta}$ thin films," *J. Appl. Phys.* **118**, 085313 (2015).
- ²⁹S. Wang, L. Wan, D. Li, X. Chen, X. Xu, Z. C. Feng, and I. T. Ferguson, "Temperature-dependent properties of graphene on SiC substrates for triboelectric nanogenerators," *Front. Mater.* **9**, 924143 (2022).
- ³⁰F. Tuinstra and J. L. Koenig, "Raman spectrum of graphite," *J. Chem. Phys.* **53**, 1126 (1970).
- ³¹L. G. Cançado, A. Jorio, E. H. M. Ferreira, F. Stavale, C. A. Achete, R. B. Capaz, M. V. O. Moutinho, A. Lombardo, T. S. Kulmala, and A. C. Ferrari, "Quantifying defects in graphene via Raman spectroscopy at different excitation energies," *Nano Lett.* **11**(8), 3190 (2011).
- ³²M. Morsin, S. Isaak, M. Morsin, and Y. Yusof, "Characterization of defect induced multilayer graphene," *Int. J. Electr. Comput. Eng.* **7**(3), 1452 (2017).
- ³³Z. Guo, Z. Ye, M. Yin, S. Dai, X. Zhang, W. Wang, and Z. Liu, "Growth of low-defect nitrogen-doped graphene film using condensation-assisted chemical vapor deposition method," *Materials* **16**, 1120 (2023).
- ³⁴L. G. Cançado, K. Takai, T. Enoki, M. Endo, Y. A. Kim, H. Mizusaki, A. Jorio, L. Coelho, R. Magalhães-Paniago, and M. Pimenta, "General equation for the determination of the crystallite size L_a of nanographite by Raman spectroscopy," *Appl. Phys. Lett.* **88**, 163106 (2006).